ELSEVIER

Journal of Non-Crystalline Solids 285 (2001) 71–78

JOURNAL OF NON-CRYSTALLINE SOLIDS

www.elsevier.com/locate/jnoncrysol

Section 2. Non-conventional processing of aerogels

Multiphased assembly of nanoporous silica particles

Hongyou Fan [a], Frank Van Swol [a], Yunfeng Lu [a], C. Jeffrey Brinker [a,b,*]

[a] *Sandia National Laboratories, Albuquerque, NM 87185, USA*

[b] *Department of Chem. and Nuclear Eng., Center for Micro-Engineered Materials, The University of New Mexico/NSF, Albuquerque, NM 87131, USA*

Abstract

Porous silica nanoparticles with well-defined mesopores and voids are described. The silica nanoparticles are produced in a rapid aerosol process. The evaporation of solvent during aerosol generation induces multiphased assembly confined to an aerosol droplet containing polystyrene spheres/silica, polystyrene spheres/surfactant/silica or microemulsions/silica. After removal of surfactants, polymer spheres, and microemulsion, the resulting materials exhibit controlled meso- and macro-porosity. TEM and nitrogen sorption isotherms have been used to characterize the porous silica particles. The silica particles templated by polystyrene spheres possess 100 nm voids. The surfactants, as secondary templates, are used to form a mesophase to interconnect the macropores. For the microemulsion-templated silica nanoparticles, the porosity and cell size are controlled by the amount of oil and the size of the swelling molecule.

PACS: 61.46+w; 78.55.Mb; 81.16.Dn

1. Introduction

Nanostructured particles exhibiting well-defined pore sizes and pore connectivity are of interest for catalysis and separation, chromatography, controlled release, low dielectric constant fillers, custom-designed pigments, and optical hosts [1–6]. Mesoporous materials with well-defined pore sizes ranging from 2 to 50 nm have been synthesized successfully via self-assembly of surfactants and inorganic metal oxides [4,7–10]. Surfactants with hydrophilic head groups and hydrophobic tails self-assemble into micelles and lyotropic mesophases in aqueous solution. The co-assembly of a surfactant and oligomeric silica results in silica–surfactant mesophases. Surfactant removal creates periodic mesoporous silica materials [11]. Different sizes of surfactants, including amphiphilic block copolymers, have been used to prepare mesoporous silica with controlled pore sizes [11,12]. Beyond changing the chain length of the hydrophobic tails to control the pore size, organic co-solvents which swell the surfactant micellar core have been used to enlarge pore size [6]. Recently, numerous studies have reported the preparation of periodic macroporous silica using polymer latex spheres [3,13–16]. The pore size depends on the size of the polymer spheres. Very recently, oil-in-water microemulsions have been used as templates to prepare periodic macroporous silica [17] or mesostructured cellular foam (MCF)

* Corresponding author. Tel.: +1-505 272 7629; fax: +1-505 272 7336.

E-mail address: cjbrink@sandia.gov (C.J. Brinker).

0022-3093/01/$ - see front matter
PII: S0022-3093(01)00434-3

materials [3,6,18,19]. The purpose of this article is to describe hierarchical porous silica nanoparticles with well-defined pore sizes (or cells) templated by polystyrene beads with or without additional surfactants, or microemulsions, through an aerosol process. Previously, we prepared mesoporous silica nanoparticles and composites through an aerosol-assisted self-assembly process [20–23]. In this paper we extend this process to synthesize hierarchical silica nanoparticles based on the multiphase assembly of polystyrene spheres/silica, surfactant/polystyrene spheres/silica, and microemulsion/silica.

2. Experimental procedures

Precursor solutions were prepared by the addition of a non-ionic surfactant (Brij-56; $CH_3(CH_2)_{15}$–$(OCH_2CH_2)_{10}$–OH, from Aldrich); or triblock copolymer (Pluronic-P123; (EO)20 (propylene oxide, PO)70 (EO)20, gift from BASF) to an acidic silica sol ($A2^{**}$) [21]. The acid concentration employed in the $A2^{**}$ synthesis procedure was chosen to minimize the siloxane condensation rate, thereby promoting facile silica/surfactant self-assembly during aerosol processing. In a typical preparation, TEOS ($Si(OCH_2CH_3)_4$), ethanol, water and dilute HCl (mole ratios: $1{:}3.8{:}1{:}5 \times 10^{-5}$) were refluxed at 60°C for 90 min. The sol was diluted with ethanol (1:2) followed by addition of water and dilute HCl. Surfactants were added in the amounts needed to achieve initial surfactant concentrations c_0 ranging from 0.004 to 0.23 M. The final reactant mole ratios (TEOS:EtOH:H_2O:HCl:surfactant) were 1:(0–22):(5–67):0.004:(0.006–0.23). Swelling agents (oil) including polypropylene glycol dimethylacrylate (PPGA, M.W. 425), and polypropylene oxide (PPO, M.W. 425 and 2000) were added in the amount of 1–10 wt% of the total weight of final sol. In the case of PPGA, a thermal initiator was added to cross-link the double bonds. TEOS was added to 3 wt% monosize polystyrene bead water solution (from Polyscience Inc., 50–100 nm) to produce silica particles with large air cells.

Silica/surfactant aerosols were generated using a commercial atomizer (Model 3076, TSI Inc., St Paul, MN, USA) operated with nitrogen as a carrier/atomization gas. This atomizer produces aerosol droplets with a size distribution characterized by a geometric standard deviation of 2 (95% of the particles have diameters between 0.25 and 4 times the mean diameter). The pressure drop at the pinhole was 2.4 atm. Particles were collected on a Teflon filter. The aerosol reactor (Fig. 1) was operated at a volumetric flow rate of 2.6 l STP min^{-1}. Under these conditions, the flow is laminar (Reynolds number at 400°C, 75) and the entrained aerosol particles experience ~3 s of drying at nominally room temperature followed by ~3 s of heating at 400°C and finally collection on a filter maintained at 80°C. The collected particles were characterized by TEM and nitrogen sorption after calcination at 425°C in air or nitrogen (heating rate, $1°C/min^{-1}$). High-resolution transmission electron microscopy (HRTEM) and electron diffraction (ED) patterns were recorded using JEOL 2010 TEM, operating at a voltage of 200 kV with a Gatan slow scan CCD camera. Nitrogen isotherms were conducted using an automated ASAP 2010 instrument (Micromeritics, Norcross, GA, USA). The calcined silica particles were degassed at 150°C for 12 h before final analysis.

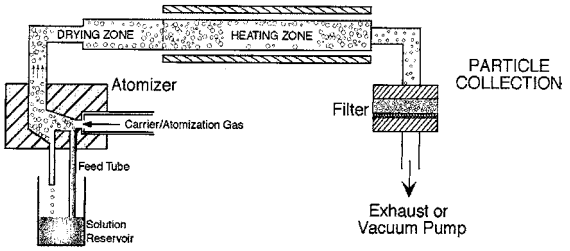

Fig. 1. Diagram of the aerosol reactor used to prepare self-assembled silica nanoparticles.

3. Results

3.1. Emulsion-templated silica particles

For the emulsion system, the initial sol was prepared by adding a swelling agent poly(propylene glycol acrylate) (designated as PPGA) to an $A2^{**}$ sol diluted 2:1 with ethanol. The silica par-

ticles were produced through an aerosol process (Fig. 1). Fig. 2 shows a series of calcined particles templated by 3 wt% P123 plus differing amounts of PPGA. Without any PPGA swelling agent, the particles form a worm-like structure with a pore size of about 7 nm, consistent with silica powders or films templated by P123 as discussed previously. After adding 3.5 wt% PPGA, we clearly see that the mesopore diameters are enlarged to ~20 nm. A further increase of PPGA to 10 wt% causes the development of a 'soccer ball'-like cellular structure composed of struts and tri-functional nodes connected into polyhedron with about a 50 nm cell size. As shown in TEM images (Fig. 2), there appears to be a silica skin surrounding the mesostructured silica particles no matter how much PPGA is added. Table 1 displays the physical properties of the three types of calcined silica particles as determined from nitrogen isotherms. It shows that the porosity increases with an increase in the amount of PPGA. The access of nitrogen molecules may be due to the presence of micropores in the silica skin.

3.2. Polystyrene bead-templated silica particles

As shown above, emulsion-templated cellular silica particles were formed through emulsion formation during the aerosol process. Polystyrene beads were used as a model to further demonstrate the emulsion templating process. Fig. 3 shows the TEM micrograph of polystyrene sphere-templated silica particles produced from a precursor solution containing about 3 wt% polystyrene beads. Similar to that of the 3.5 wt% PPGA emulsion system, spherical air voids are formed within the silica particles. Whereas the soft emulsion formed polyhedron silica frames when the PPGA concentration was increased to 10 wt%, hard polybeads always template spherical voids. To assess the porosity of the final particles we performed Monte Carlo (MC) simulations of N monodisperse hard spheres confined to a hard spherical container [24]. To generate the starting configuration spheres of diameter σ were placed randomly inside a container of radius R and volume V. The starting value of V was large and hence the packing fraction (ϕ) was around

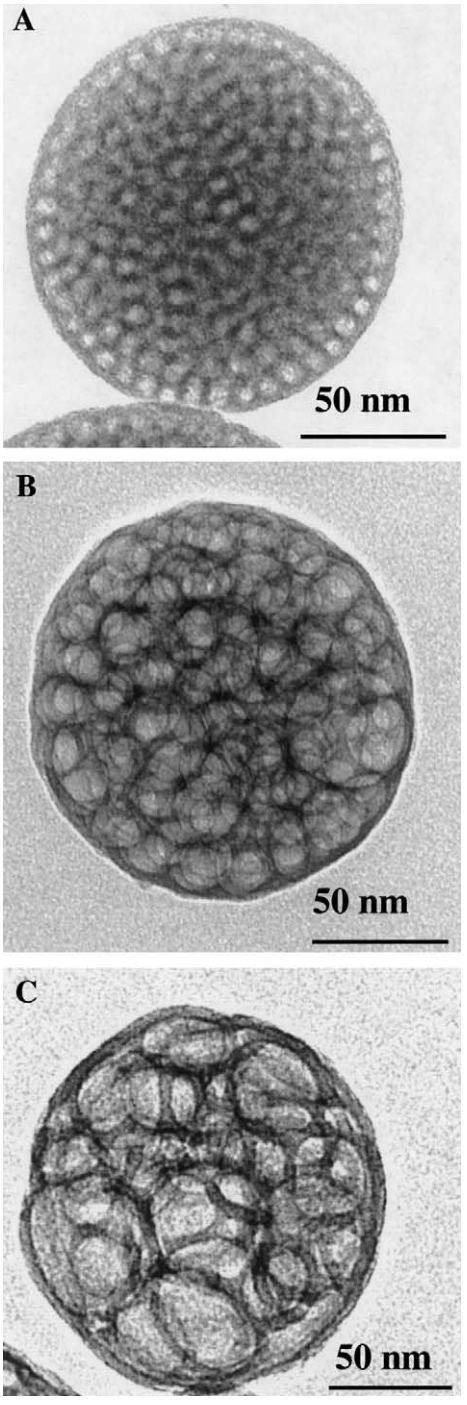

Fig. 2. TEM images of aerosol-generated mesoporous silica particles templated by 3 wt% P123 with/without co-solvent: (a) 3 wt% P123; (b) 3 wt% P123 + 3.5 wt% PPGA; (c) 3 wt% P123 + 10 wt% PPGA.

Table 1
Physical and chemical properties of mesoporous silica particles templated by P123 and microemulsions

Samples	Surface area (m^2/g)	Pore size (Å)	Pore volume (cm^3/g)
3% P123	428	54	0.58
3% P123 + 3.4% PPGA	190	127	0.60
3% P123 + 10% PPGA	244	144	0.98
4% P123 + PPO (425)	323	65	0.53
4% P123 + PPO (2000)	320	110	0.88

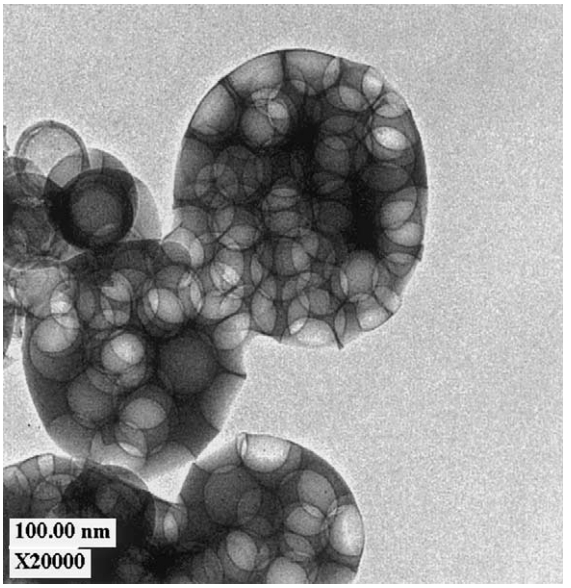

Fig. 3. TEM image of silica particles templated by polystyrene beads.

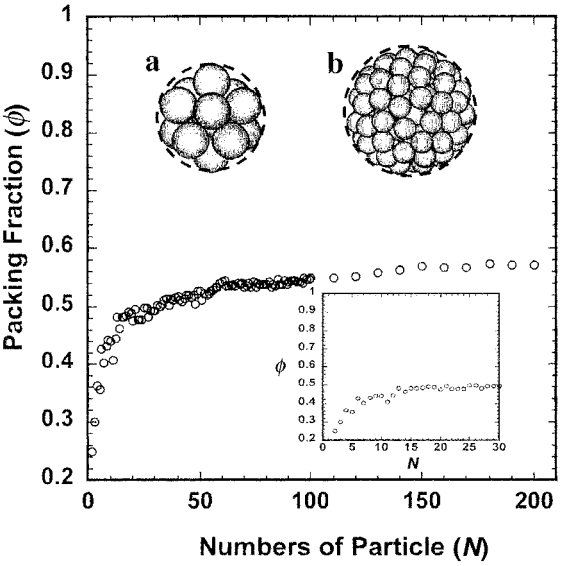

Fig. 4. MC simulations of packing fractions of N monodisperse hard spheres confined to a hard container: (a) $N = 13$, showing icosahedral structure; (b) $N = 100$.

0.01. Fig. 4 shows the packing fractions of monodisperse hard spheres in a hard spherical container where

$$\phi = \frac{\pi N \sigma^3}{6V}.$$

Fig. 5(a) shows the TEM micrograph of polybead/surfactant-templated silica particles produced with a precursor solution containing 3 wt% polybeads and 1 wt% Brij-56. For Brij-56 surfactant, we found that micelles are formed at low surfactant concentration (<1 wt%). In Fig. 5(a), we can clearly see the micelles formed within the silica skin layer. The dimension of these micelles is about 45 Å, which is consistent with the previous results from the formation of micelles within films. These micelles are randomly isolated within the silica wall as shown. Nitrogen sorption isotherms (see Fig. 6(a)) show a large desorption hysteresis. This is because micelles do not form a continuous mesophase within the silica wall. In order to form a continuous mesophase, 3 wt% Brij-56 was added to the precursor containing 3 wt% polybeads. The TEM image in Fig. 5(b) shows the microstructure of the calcined samples. A secondary periodic mesophase is formed within the silica wall. Fig. 6(b) shows type IV isotherms containing no desorption hysteresis loop. The pore size is about 40 Å. Table 2 summarizes the detailed physical properties of these silica particles.

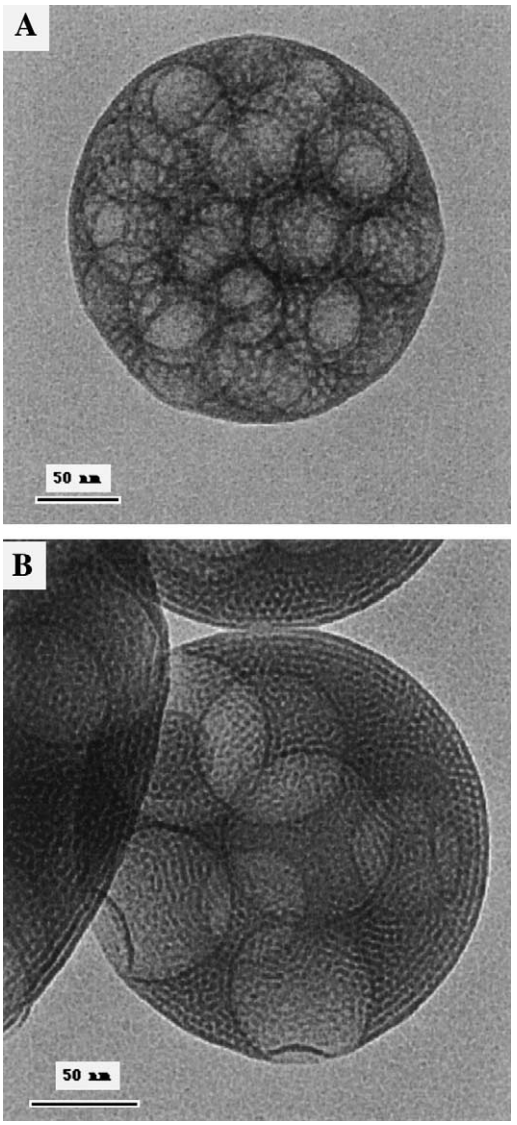

Fig. 5. TEM images of silica particles templated by polystyrene beads with (a) 1 wt% Brij-56 and (b) 3 wt% Brij-56.

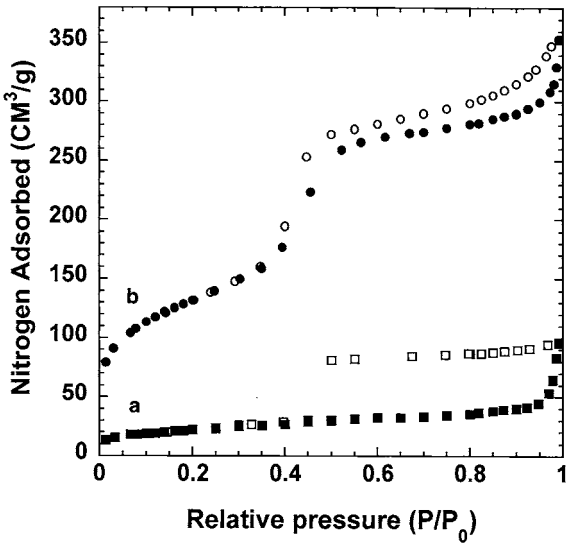

Fig. 6. Nitrogen isotherms of silica particles templated by polystyrene beads and (a) 1% Brij-56, (b) 3% Brij-56 (adsorption, solid symbols; desorption, blank symbols).

Table 2
Physical and chemical properties of silica particles templated by polystyrene beads (PB) and Brij-56

Samples	Surface area (m^2/g)	Pore size (Å)
PB + 1% Brij-56	75	40
PB + 3% Brij-56	476	40
PB + 4% Brij-56	480	39

4. Discussion

Previously we have synthesized mesoporous silica nanoparticles and composites based on the co-assembly of surfactant–silica through an aerosol-assisted self-assembly process. The process starts with a homogeneous solution of soluble silica and surfactant prepared in an ethanol/water solvent with an initial surfactant concentration c_0 much less than the critical micelle concentration (c.m.c.). In a continuous, 6-second process, the aerosol particles are dried, heated and collected. Preferential alcohol evaporation during drying enriches the particles in surfactant, water and silica, inducing micelle formation and successive co-assembly of silica–surfactant micellar species into liquid–crystalline mesophases. Here we extend this process to a new system in which we use solid soft microemulsion and solid polystyrene beads as templates to produce nanoporous silica particles with adjustable meso- or macro-porosities.

For the soft microemulsion system, preferential solvent evaporation induced the formation of

microemulsion/silica during aerosol droplet production; alcohol, which destroys the microemulsion because of its tendency to mix both oil and water, evaporates quickly into air. The evaporation concentrates the droplets in water, surfactant, oil (PPGA) and silica, which then form an oil-in-water microemulsion, a soft template. Simultaneously, silica condensation solidifies the droplets containing the microemulsions. Subsequent calcination leads to the formation of silica 'soccer balls' containing large voids. In the absence of PPGA, particles with worm-like mesostructure are formed with a 7-nm dimension pore that is in agreement with the previous results [12,23]. The polyhedral morphology may be due to the packing forces between the bubbles. Increasing the concentration of PPGA in the precursor solution leads to an increase in cell size and total pore volume.

For the solid polystyrene bead system, the polystyrene beads themselves serve as templates. The self-assembly is confined to an aerosol droplet containing silica/water/polystyrene beads. Silica condensation freezes the self-assembled droplet. After calcination, the pores within the silica particles retain the size and spherical geometry of the corresponding polystyrene beads. For the MC simulations of packing fraction of polystyrene beads within a silica particle, the drying process of the gel was mimicked by gradually shrinking the container. This can be conveniently accomplished by employing the familiar constant pressure (p) or (NpT) ensemble simulation method. Setting the value of p to a very large value, one forces the spheres to be quickly compressed, ending up with a close-packed configuration that corresponds to rapid drying. Depending on the value of N the result of such a large compression can be either a regular or random close packing. For example, for very small N ($N < 7$, say) it is not difficult to establish that there is a unique structure or stacking of spheres inside a spherical container that corresponds to the maximum possible ϕ. Moreover, given the smallness of N it is also expected that the system will indeed end up in these structures as there is very little opportunity to get trapped in other states. Some other special values of N are known to lead to familiar structures, including $N = 13$, which produces a very efficient icosahedral packing (Fig. 4, inset a). This is similar to the problem of small crystalline clusters, where certain so-called magic number clusters occur that are distinguished from other N by their low energy. The reason for the occurrence of magic numbers is indeed closely related to the problem at hand, as low energies require efficient high density packings that are globular. In contrast, for large N, the situation can be quite different. For $N, R \to \infty$ the optimum packing is crystalline and known (i.e. an fcc or hcp or any hybrid of hcp and fcc). Indeed, from experiments on colloidal suspensions we know that crystal growth can be observed as long as the polydispersity is small and the compression or sedimentation is slow. However, both simulations and colloidal experiments show that *fast* compressions will typically bypass crystallization and lead to non-crystalline random close-packed (RCP) structures. For $N, R \to \infty$, the final RCP packing fraction observed for monodisperse systems is $\phi_{\mathrm{PX\Pi}} = 0.638$. Slightly larger values (e.g. 0.645) result when there are small crystallites present. Polydisperse systems have larger values for $\phi_{\mathrm{PX\Pi}}$ that can approach unity. In Fig. 4, we have collected the results for $\phi_{\mathrm{PX\Pi}}$ for a large number of simulations where N varies from 1 to 200.

In order to build the interconnection between these large air cells, we added surfactants into the system. For low concentration of surfactant (<1 wt%), the TEM images show a formation of surfactant micelles, 4.5 nm in diameter, which are randomly dispersed within the silica skin layer. The nitrogen isotherms show a large hysteresis, indicating poor interconnectivity among the micelles. In order to form an interconnected pore system within the particles, we increased the surfactant concentration in the starting solution. As shown in Fig. 5(b) in addition to the large voids templated by polystyrene beads, a secondary periodic mesophase is formed within the silica wall between the voids. Nitrogen isotherms (Fig. 6(a)) show a disappearance of the hysteresis loop, confirming the interconnection within a particle. We believe that this process is similar to that of the recently demonstrated formation of mesostructured thin films [21,22]; preferential alcohol evaporation during drying enriches the films in surfactant, water and silica, inducing micelle

formation and successive co-assembly of silica–surfactant micellar species into liquid–crystalline mesophases. The subsequent 'growth' of the liquid–crystalline domains from both air/film and film/substrate interfaces towards the center of the film results in a mesostructured silica film. In the polystyrene beads/surfactant/silica system, the secondary mesophase grows from both the air/liquid and polystyrene spheres/liquid interfaces toward the interior of the aerosol droplet. For the emulsion system, surfactants were added to support and stabilize the formation of emulsion. However, in the polybead system, the surfactant performs as a secondary template and forms a mesophase within the aerosol droplet. Nitrogen isotherms showing almost no hysteresis indicate a good connectivity between the large voids. This further confirms the formation of mesopores within the silica wall.

5. Conclusions

We have synthesized nanoporous silica particles with well-defined pore structures and voids through an aerosol-assisted self-assembly process. This process results in hierarchically organized pore structures templated by surfactant, polystyrene spheres, and oil-in-water microemulsions. The different length scale characteristics can be tailored by adding different amounts of swelling agent (oil) in the microemulsion system or surfactants to the polystyrene bead system. For the microemulsion system, the surfactant was added to form and stabilize the emulsion. The void inside the silica particles depends on the emulsion size. However, for the polystyrene bead system, the polybeads themselves perform as structure templates. Added surfactants serve as secondary templates and result in dual meso- or macro-porosities in silica particles. MC simulations indicated a maximum porosity of $\sim$64% for the polystyrene bead-templated silica particles. These types of hierarchical silica particles could be used in applications as large molecule catalysis and separation, low k dielectric fillers, hosts for biomolecules, and chromatographic supports.

Acknowledgements

This work was partially supported by the UNM/NSF Center for Micro-Engineered Materials and the Department of Energy Basic Energy Sciences Program, Sandia National Laboratories Lab-Directed Research and Development Program. TEM investigations were performed in the Department of Earth and Planetary Sciences at the University of New Mexico. We thank BASF for providing Pluronic surfactants. Sandia National Laboratories is a multi-program laboratory operated by Sandia Corporation, a Lockheed Martin Company, for the US Department of Energy under Contract DE-AC04-94AL85000.

References

[1] M. Antonietti, B. Berton, C. Goltner, H.P. Hentze, Adv. Mater. 10 (1998) 154.
[2] P.J. Bruinsma, A.Y. Kim, J. Liu, S. Baskaran, Chem. Mater. 9 (1997) 2507.
[3] B.T. Holland, C.F. Blanford, T. Do, A. Stein, Chem. Mater. 11 (1999) 795.
[4] G.A. Ozin, Chem. Commun. (2000) 419.
[5] S. Schacht, Q. Huo, I.G. Voigt-Martin, G.D. Stucky, F. Schuth, Science 273 (1996) 768.
[6] D.Y. Zhao, P.D. Yang, B.F. Chmelka, G.D. Stucky, Chem. Mater. 11 (1999) 1174.
[7] S. Biz, M.L. Occelli, Cat. Rev.–Sci. Eng. 40 (1998) 329.
[8] U. Ciesla, F. Schuth, Micro. Meso. Mater. 27 (1999) 131.
[9] M. Raimondi, J. Seddon, Liquid Cryst. 26 (1999) 3.
[10] J.Y. Ying, C.P. Mehnet, M.S. Wong, Angew. Chem. Int. Ed. 38 (1999) 56.
[11] C. Kresge, M. Leonowicz, W. Roth, C. Vartuli, J. Beck, Nature 359 (1992) 710.
[12] D.Y. Zhao, Q.S. Huo, J.L. Feng, B.F. Chmelka, G.D. Stucky, J. Am. Chem. Soc. 120 (#24) (1998) 6024.
[13] S.H. Park, Y.N. Xia, Chem. Mater. 10 (1998) 1745.
[14] O.D. Velev, A.M. Lenhoff, E.W. Kaler, Science 287 (2000) 2240.
[15] O.D. Velev, E.W. Kaler, Adv. Mater. 12 (2000) 531.
[16] O.D. Velev, A.M. Lenhoff, Curr. Opin. Colloid Int. Sci. 5 (2000) 56.
[17] A. Imhof, D.J. Pine, Nature 389 (1997) 948.
[18] W.P. Schmidt, W.W. Lukens, P.D. Yang, D.I. Margolese, J.S. Lettow, J.Y. Ying, G.D. Stucky, Chem. Mater. 12 (2000) 686.
[19] W.P. Schmidt, C.J. Glinka, G.D. Stucky, Langmuir 16 (2000) 356.
[20] C.J. Brinker, Y.F. Lu, A. Sellinger, H.Y. Fan, Adv. Mater. 11 (1999) 579.

[21] H.Y. Fan, Y.F. Lu, A. Stump, S.T. Reed, T. Baer, R. Schunk, V. PerezLuna, G.P. Lopez, C.J. Brinker, Nature 405 (2000) 56.
[22] Y. Lu, R. Ganguli, C. Drewien, M. Anderson, C. Brinker, W. Gong, Y. Guo, H. Soyez, B. Dunn, M. Huang, J. Zink, Nature 389 (1997) 364.
[23] Y. Lu, H. Fan, A. Stump, T.L. Ward, T. Reiker, C.J. Brinker, Nature 398 (1998) 223.
[24] M.P. Allen, D.J. Tildesley, in: Computer Simulation of Liquids, Oxford University, Oxford, 1989.